A Parametric Wind Tunnel Test on Rotorcraft Aerodynamics and Aeroacoustics (HELISHAPE) - Test Procedures and Representative Results

K.-J. Schultz, W. Splettstoesser, B. Junker and W. Wagner
DLR, Braunschweig, Goettingen, Germany

E. Schoell
ECD, Ottobrunn, Germany

G. Arnaud
ECF, Marignane, France

E. Mercker and K. Pengel
DNW, Emmeloord, The Netherlands

D. Fertis
ALFAPI, S.A., Athens, Greece

Abstract

In the framework of a major European cooperative research programme on rotorcraft aerodynamics and acoustics (HELISHAPE) a parametric model rotor test was conducted in the open test section of the DNW using the MWM test rig of DLR and a highly instrumented model of a fully articulated ECF rotor equipped with blades of advanced design and two exchangeable blade tips. One set of blade tips (7A) was of rectangular, the other one (7AD1) of swept-back parabolic/anhedral shape. The objectives of this experimental research were to evaluate noise reduction techniques (conceptionally by variation of rotor speed, dedicated tip shapes and advanced airfoils as well as operationally by identifying low noise - BVI-minimizing- descent procedures) and to validate the partners aerodynamic and aeroacoustic codes. A comprehensive set of simultaneous acoustic and aerodynamic blade surface pressure data as well as blade dynamic and performance data was measured. In addition, valuable information on the tip-vortex geometry and blade-vortex miss distance was obtained by LLS flow visualization. The experimental equipment, the test procedures, and the test matrix are briefly described. A survey on the main results is presented and the trends of the most important parameter variations for both rotors are discussed.

Introduction

Helicopter rotor noise - especially the characteristic impulsive noise at high speed level flight and moderate descent - is known to be highly annoying and intrusive. Therefore rotor noise will be one of the major design parameters for the next generation of quieter rotorcraft. This requires more accurate aeroacoustic prediction tools. But, the development or improvement of numerical codes to accurately predict and eventually control rotor noise will only be possible by a better physical understanding of the complex rotor aerodynamic, dynamic, and acoustic phenomena.

Since the early eighties experimental and theoretical studies on rotor noise were intensified in the US and in Europe, often in the framework of international cooperative rotor aeroacoustic research programmes. Important steps to improve this understanding were made by comprehensive model rotor tests with simultaneous measurements of blade pressures and acoustics which provided an improved physical insight into the close relationship between the blade aerodynamics and the radiated noise. A "benchmark" experiment was the 1/7-scale AH-1/OLS model rotor test in the DNW in 1982 [Refs. 1, 2]. Inspired by the high quality AH-1/OLS test results several cooperative tests were executed in the DNW characterized by simultaneous blade pressure and acoustic measurements, employing for instance a 1/5-scaled Boeing 360 model [Ref. 3] or a Sikorsky 1/5.7-scaled technology rotor model [Ref. 4]. During early experiments with a 1/2.5-scaled BO-105 model rotor in the DNW only acoustic measurements were possible [Ref. 5]. BO-105 main/tail rotor model tests using an instrumented tail rotor blade were performed in the DNW in 1988/89 [Ref. 6]. A high quality data base of simultaneously measured acoustic and blade pressures for a hingeless helicopter main rotor was acquired in the DNW within the cooperative European research programme HELINOISE [Ref. 7], employing a 40%-geometrically and dynamically scaled and highly instrumented main rotor model of the BO-105 helicopter.

In order to enable the continuation of the aeroacoustic research work aiming at a better public acceptance of today's and future helicopters a major cooperative research programme on rotorcraft aerodynamics and aeroacoustics under the acronym HELISHAPE had been initiated by the European Union. The objectives of the programme were the improvement of aerodynamic and aeroacoustic prediction capability for more advanced blades of a fully articulated rotor as well as the investigation of helicopter noise reduction measures in the framework of a quiet helicopter feasibility study. To accomplish these goals six major tasks have been identified including theoretical and experimental work. One of these main tasks, Task 5 "parametric wind tunnel tests", was established in order to validate the aerodynamic and aeroacoustic simulation codes and to evaluate noise palliatives.

Whereas in HELINOISE conventional blades were tested, within the parametric wind tunnel tests of HELISHAPE rotor blades of advanced airfoil design and two exchangeable blade tips were chosen for investigation. The major objectives of this experimental research were (1) to evalu-

ate noise reduction measures (conceptionally by variation of rotor speed, dedicated tip shapes and advanced airfoils as well as operationally by identifying low noise - BVI-minimizing - descent procedures) and (2) to validate the partners' aerodynamic and aeroacoustic codes developed or improved in other HELISHAPE tasks.

This paper describes the test procedures applied and presents a survey on the main results. The findings for the two different tip shapes are compared and the trends of the most important parameter variations are discussed. The aeroacoustic improvements of the 7AD1 blade tip compared to the rectangular 7A tip are investigated with respect to Blade-Vortex Interaction (BVI) noise and with respect to High-Speed (HS) noise. The strong correlation of the blade aerodynamic characteristics and the acoustic radiation are demonstrated.

Experimental Equipment

Wind Tunnel

The test was conducted in the open test section of the German-Dutch Wind Tunnel (DNW) located in the North East Polder, The Netherlands, which is known as one of the best aeroacoustic test facilities in existence. The DNW is a subsonic, atmospheric, closed circuit wind tunnel with three interchangeable, closed test section configurations and one open configuration. The open jet configuration used for this aeroacoustic test, employs an 8 x 6 m^2 contraction section and a 19 m-long test section, surrounded by a large anechoic hall of about 30 000 m^3 lined with absorptive acoustic wedges (cut-off frequency of 80 Hz). The tunnel has low background noise and excellent fluid dynamic properties, described in Refs. 8 and 9.

Model Rotor Test Stand

The Modular Wind-Tunnel Model (MWM) rotor test stand, documented in Reference 10, was employed to drive the model rotor. The test set-up equipped with the 7A rotor (a) and the 7AD1 rotor (b) together with the inflow microphone traverse is shown installed in the DNW open test section in Figure 1. The MWM test stand was already used for the HELINOISE test campaign (Ref. 7). The test stand consists of three major sub-systems: the hydraulic rotor drive system (130 kW), the rotor balance system using separate measuring elements for static and dynamic load components, and the rotor control system comprising the swashplate and three computer-controlled electrodynamic actuators providing collective and cyclic pitch control. The MWM was housed within an acoustically insulated fiberglass fairing shaped like a scaled-down helicopter fuselage and designed to largely reduce the hydraulic drive noise of the 9-piston axial hydraulic motor. The MWM test rig was supported by the computer-controlled, hydraulically actuated model sting support mechanism of the DNW.

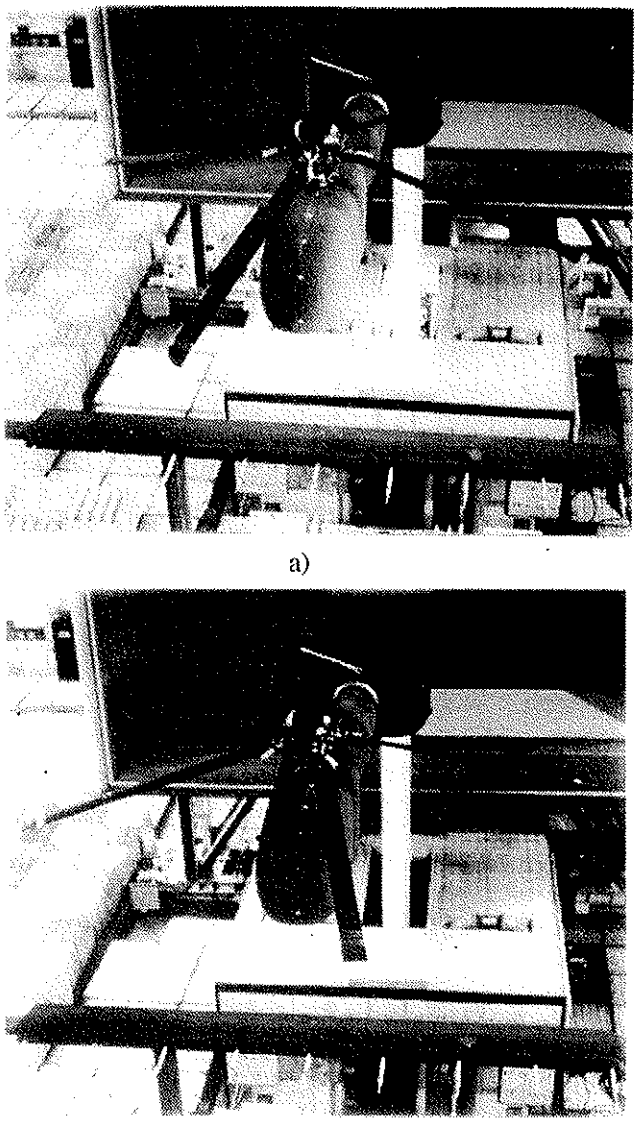

a)

b)

Fig. 1 Test set-up installed in the DNW open test section a) with 7A rotor, b) with 7AD1 rotor

Model Rotor and Instrumentation

The tested model rotor was a fully articulated rotor of modern airfoil design and highly instrumented. The rotor and a suitable rotor hub was provided by partner ECF. The adaptation of the hub to the MWM test rig was provided by partner DLR. The model rotor featured advanced blade design and exchangeable blade tips, which were pressure instrumented as well. One set of blade tips (7A) was of rectangular, the other one (7AD1) of parabolic/anhedral swept-back shape. The rotor blades were formed of ONERA OA209 and OA213 airfoils. The 4.2 m diameter rotor was equipped with a total of 118 (117 operational) absolute pressure transducers of the piezoresistive type (Kulite XCQ) and with 28 (27 operational) strain gauges.

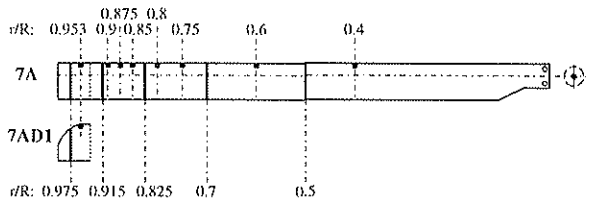

Fig. 2 Blade pressure sensor distribution

The pressure sensor distribution is illustrated in Figure 2. The pressure transducers were distributed on all four blades to measure the chordwise pressure distribution in five sections (0.5, 0.7, 0.82, 0.92 and 0.975 R) with about 20 sensors per section and furthermore the radial distribution near the leading edge (2% chord, upper and lower side) on 6 additional radial sections between 0.4 and 0.95 R. Blade 1 was only instrumented on the lower side, blades 2 and 3 only on the upper side, and blade 4 only along the leading edge at 2% chord.

The strain gauges were distributed on blades 1 to 3 to measure blade flapping, in-plane, and torsional moments and deflections.

The output signals of the 118 pressure transducers as well as the additional measurement signals from the rotor were pre-amplified by miniaturized amplifiers in the rotating frame and transmitted via a 256-channel slipring system to the fixed frame.

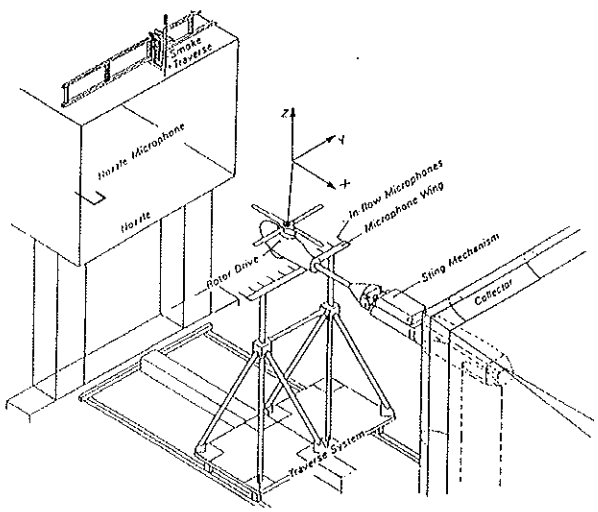

Fig. 3 Test set-up for aeroacoustic measurements

A dynamic frequency response calibration was performed of each pressure transducer prior to the test. The steady-state pressure sensitivity calibration was conducted during the DNW entry with a special pressure sealed tube. To improve the accuracy of the blade pressure results a special computer controlled temperature compensation of the sensors was applied for the HELISHAPE tests.

Acoustic Instrumentation

The acoustic instrumentation consisted of a linear inflow microphone array mounted on a ground based traverse system with a maximum range of 11 m in flow direction. The principle arrangement of the traversing gear inside the testing hall is depicted in Figure 3. The microphone array was shaped like a horizontal wing with its span normal to the flow and covered with open-cell foam to reduce reflections. Eleven microphones were arranged symmetrically with respect to the tunnel centerline and equally spaced 0.54 m apart. The array vertical position was usually 2.3 m (1.15 R) below the rotor hub. One additional microphone was installed on the wind tunnel nozzle exit near the tunnel centre line on the advancing side with respect to the rotor. This microphone position was chosen to obtain acoustic data radiated in the rotor plane, most important for hover and high-speed forward flight.

The microphones were 1/2-inch pressure-type condenser microphones (B&K 4134) equipped with "bullet" nose cones. The microphone holders employed a soft vibration-isolation mounting. Standard microphone calibration procedures were applied.

The traverse mechanism was powered by a variable-speed dc electric motor. Control and position (referenced to the rotor hub) was established with a servo position controller. Position accuracy was about 2 mm. The traversing speed was programmable in a range between 0 and 150 mm/s.

Laser Light Sheet (LLS) Flow Visualization Technique

The LLS flow visualization technique (Ref. 11) enabled (1) to visualize tip vortex sections in order to gain qualitative information on the vortex structure and (2) to attain quantitative information on the geometry of tip-vortex segments and on the blade-vortex miss distance.

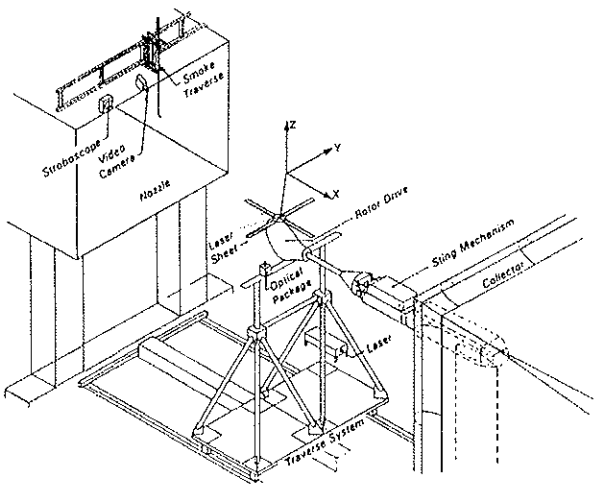

Fig. 4 Test set-up for flow visualization by LLS

The test set-up as used for the descent flight conditions is illustrated in Figure 4. Employing a 5 W argon laser and an optical package mounted an the microphone traverse a continuous thin light sheet was erected normal to the rotor

plane and approximately vertical to the vortices to be visualized. For flow visualization oil smoke generated by a remotely controlled traversable smoke generator, was introduced into the flow by a smoke probe. For the LLS measurements at descent conditions the smoke probe was mounted at the wind tunnel nozzle. When the smoke probe was correctly adjusted, the smoke particles within the vortex section were illuminated by the laser light such that the vortex center could be identified. This image was recorded by a fast motion video camera, mounted on the top of the nozzle and triggered by a 512-per-revolution blade position signal of the rotor.

In order to evaluate the blade-vortex miss distance a high power stroboscopic light source was used to illuminate the rotor blade. The light source was also triggered by the 512-per-revolution signal of the rotor. Thus, the vortex and the blade could be visualized at the same time. Furthermore, in order to determine the position of the vortex in space a grid was recorded with the same video camera (after the rotor and the wind tunnel were turned off). The grid was placed in the plane of the laser light sheet. Later, the recorded picture was digitized and used as an overlay on the actual flow recording, which then provided the relative position of the vortices and the blade. By either moving the light sheet or the smoke probe, a number of discrete vortex core positions for a fixed blade position (at descent conditions at 55 degrees azimuth) was determined and used to reconstruct segments of the vortex trajectories.

The laser light sheet test set-up was somewhat different for the measurements at hover conditions. The light sheet was erected at an azimuth angle of 270 degrees and the smoke was introduced directly near the rotor tip with a special triple smoke probe.

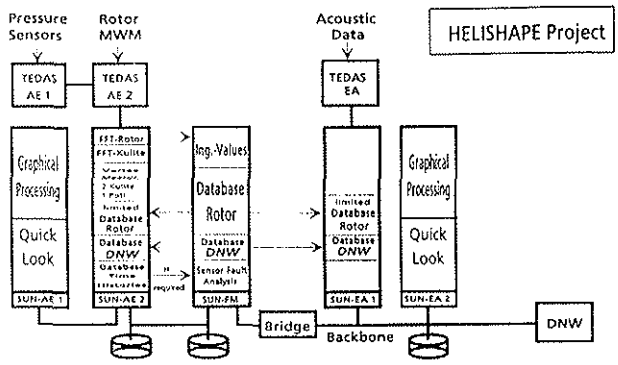

Fig. 5 Complete data acquisition architecture

Data Acquisition and Analysis

A scheme of the complete data acquisition architecture necessary to acquire simultaneous sets of blade pressure and acoustic data complemented by the related rotor performance and wind tunnel data collected in a common data base is diagrammed in Figure 5. The individual acquisition systems of DNW and DLR were all computer controlled and linked together ensuring easy data transfer. Synchronization between the systems was established by blade position reference signals (1/rev, 2048/rev) supplied by a rotor azimuth angle encoder.

Rotor Performance and Blade Pressure Data

The rotor data acquisition system acquired both the rotor performance and control parameters from the rotating and non-rotating frame as well as the blade pressure and strain gauge data from the rotating blades. This high-frequency, multi-channel system (10 kHz, 352 channels) consists of specially configured "transputer-based expandable data acquisition systems (TEDAS)" controlled by modern standard workstations (Ref. 12). The TEDAS modules developed by partner DLR have successfully been used in the HELINOISE project. Data pre-processing with TEDAS was very time-efficient since all transputer modules were working in parallel, so that shortly after the test the measurement results were available for display and plotting. The raw data of 60 rotor revolutions, the averaged, and pre-processed data were finally stored on digital tape for later evaluation.

The rotor performance data were obtained from the rotating and fixed systems of the DLR test stand control system. The rotating system acquired the signals of 27 strain gauges on the rotor blades (flapwise bending moments, edgewise bending moments and torsional moments) of strain gauges on the control rods (pitch link forces), on the rotor shaft (bending moment) and the signals of the blade root potentiometer (blade pitch angle). The fixed system signals were acquired from the displacement transducers, the static and dynamic balance transducers, the shaft torque transducer, the shaft rpm encoder (360-per-revolution), and the shaft position encoders (once-per-revolution and 2048-per-revolution). All rotor signals (rotating and non-rotating except the blade pressure data) and the wind tunnel data were processed by the rotor test stand workstation. This workstation also provided continuous on-line display of the rotor control parameters: hover tip Mach number, thrust, hub moments, blade bending, and pitch link loads. Details of the rotor data processing are given in Reference 13.

The blade pressure data were acquired and stored in terms of instantaneous and averaged time histories for one revolution (azimuthal distribution) as well as in terms of averaged spectra and spectra of the averaged time histories. The digitized signals of the 117 operational blade pressure sensors were processed on a separate workstation for quick-look graphic presentation of pressure time histories and chordwise pressure distributions. Because the pressure

transducers were distributed on four different blades the prevailing phase differences between the transducers, which belong to the same radial section but were installed in different blades, had to be accounted for.

Local blade airloads were calculated by chordwise integration of the blade pressure coefficients at each radial section. Furthermore for convenient visual interpretation of the physical processes, azimuthal and radial distributions of the unsteady part of the blade pressures near the leading edge (2% chord) were provided for the entire rotor area instrumented.

Acoustic Data

The 14-channel analog acoustic data acquisition system of DLR, proven in a number of DNW entries, was used to acquire the acoustic signals from the microphone array and the nozzle microphone. Frequency response of the complete analog acoustic measurement system was investigated in detail prior to an earlier DNW entry (Ref. 5). In parallel to the analog data recording (used as backup), a modern digital data acquisition system was employed for on-site quick-look monitoring and convenient off-line analysis. This digital acoustic data acquisition system was configured similar to the rotor data acquisition system consisting of a high frequency (>20 kHz), multichannel TEDAS system controlled by a modern workstation.

A very time-efficient and sufficiently exact method was chosen to acquire the acoustic data in a large plane below the rotor. Termed "on-the-fly" data acquisition technique, the inflow microphone array was moved slowly (33 mm/s) and continuously over the measuring range of typically 4 R (2 R downstream and 2 R upstream of the rotor center). The measuring range was depending on the test condition. For positive shaft angles the range downstream of the rotor hub was slightly restricted to avoid collision of the microphone traverse with the model suspension. The microphone signals were recorded continuously together with the streamwise microphone position signal and the synchronizing signals on analog tape.

For online analysis of the noise radiation directivity and quality control purposes the acoustic data were digitally acquired every half meter in streamwise direction providing typically 178 acoustic measurement points for each rotor condition. At each pre-selected streamwise position the acoustic data acquisition system was started and the microphone signals (11 array microphones, 1 nozzle microphone) were conditionally sampled at a rate of 2048/rev over a period of 30 rotor revolutions (1.7 seconds), giving a useful frequency range of about 18 kHz.

The maximum angular displacement of the microphone array during the 1.7-second data acquisition period was 1.9° and it was verified (by comparison with instantaneous data, Ref. 7) that the ensemble averaged acoustic data were not noticeably affected. The travel time (about 18 seconds) between the pre-selected acquisition locations was used to transmit the digitized data to the host computer for subsequent analysis, display, and plotting.

For each acoustic measurement point the ensemble averaged sound pressure time histories as well as averaged narrow band power spectra (via FFT) were calculated. The data were further evaluated in terms of A-weighted levels as well as of bandpass summary levels comprising low-frequency levels calculated from the 2nd to the 10th blade passage frequency (bpf) harmonic (an approximate measure for thickness and high speed noise) and mid-frequency levels computed from the 6th to the 40th bpf harmonic (a representative measure for BVI impulsive noise). Finally, the results were presented in terms of isobar contour plots illustrating the noise radiation field of interest below the rotor.

Test Programme

The HELISHAPE test plan was based on the flight envelope of a modern representative helicopter and comprised hover conditions, descent, climb, and level flights conditions.

The test programme started with a pre-test phase comprising, calibrations, background noise tests at different wind tunnel speeds, and measurements of the aerodynamic model hub forces which had to be known in advance for the selected rotor force trim procedure.

The main phase consisted of aerodynamic and aeroacoustic measurements for both tip shapes. At first, some hover test cases were performed with variation of the tip Mach number ($0.573 \leq M_H \leq 0.661$) and variation of the thrust coefficient($0.00058 \leq C_T \leq 0.00853$).

The simulated flight tests conditions were defined by the flight speed, the flight path angle and the specified thrust condition. The trim forces (lift and propulsive forces) for the rotor trim were determined following a special force trim procedure (described below). For investigation of blade-vortex interaction (BVI) noise a descent flight with -6 degrees path angle and a flight speed of 35 m/s was selected as nominal (BVI) flight condition. Based on this nominal descent flight condition, a lateral and a longitudinal non-zero flapping trim variation was performed followed by a flight path angle variation from -2 degrees up to -10 degrees at a constant flight speed of 35 m/s and a flight-speed variation (25 to 45 m/s) at the constant nominal glide path angle of -6 degrees. Furthermore, tip-speed variations ($0.573 \leq M_H \leq 0.661$) and thrust variations ($0.00682 \leq C_T \leq 0.00851$) as well as combined flight-path and flight-speed variations were performed. Only one climb condition (6 degrees glide path and 35 m/s flight speed) with tip-speed variation was included in the test matrix because the main rotor noise levels at climb are very low due to the absence of wake interference effects.

At level flight condition a flight-speed variation between 35 and 76 m/s was conducted followed by tip-speed variations at 60, 70 and 76 m/s flight speed and a thrust variation at 60 m/s flight speed.

LLS flow visualization was performed for descent flight and hover conditions. The laser light sheet flow visualization was chosen to determine the blade tip vortex geometry, i.e. vortex core position and blade-vortex miss distance for validation of aerodynamic wake prediction codes. LLS was exclusively applied on the advancing side (due to time limitations) at four different descent conditions and one thrust variation for both tip shapes. At hover condition a thrust and a tip-speed variation were investigated.

WT Simulation of Flight Conditions

Force Trim Procedure

To simulate free flight conditions in the wind tunnel the model rotor has to be trimmed to match the full-scale tip Mach number, advance ratio, thrust coefficient, and tip-path-plane angle. Because during the HELISHAPE test two aerodynamically different rotor designs with different drag were to compare, the more elaborate force trim procedure was chosen. The objective was to simulate an actual helicopter with given mass, given fuselage drag area, flying at a given velocity and a given flight path slope. Therefore, the rotor was trimmed to match specified aerodynamic forces, i.e. rotor lift and drag coefficients (lift- and propulsive forces) were kept as close as possible to predefined values. Such coefficients comprise only blade aerodynamic forces. Forces developed by the rotor hub and blade roots, which are not representative for any helicopter, were subtracted. The trim forces of the wind tunnel model were also defined as aerodynamic forces. Thus, the trim forces were determined by means of the measured hub forces, the modeled drag forces, and the prescribed rotor thrust.

Wind Tunnel Correction

In the wind tunnel the direction of the flow velocity vector in front of the rotor disc is influenced by the jet shear layer in the open test section and by the test section and model dimensions. To account for the resultant flow deflections, a rotation of the aerodynamic coordinate system about a correction angle $\Delta\alpha$ was performed according to a formulation of Brooks (Ref. 14).

Precalculations

In order to conduct the tests in the shortest possible time, it was important to start each trim procedure with initial values for control parameters which were reasonably close to the final values that exactly satisfy the constraints. A numerical rotor model was used to prescribe these initial values. The precalculations also provided an estimate of the shaft power, so it could be verified in advance that each test point could actually be achieved with the existing drive motor. The precalculations were performed by partner ECF, using the R85S code, version 3.0.

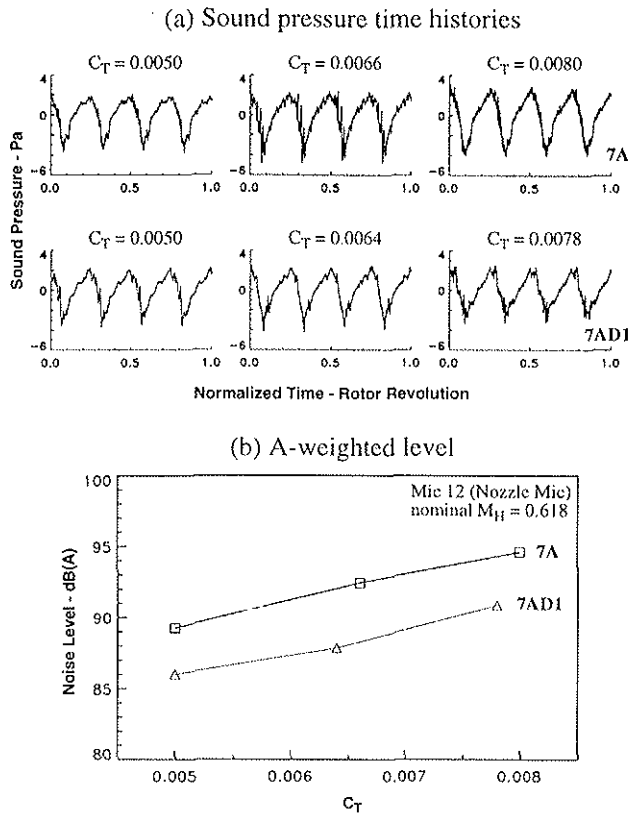

Fig. 6 Comparison of in-plane noise time histories (a) and A-weighted levels (b) for 7A and 7AD1 rotor at hover thrust variation

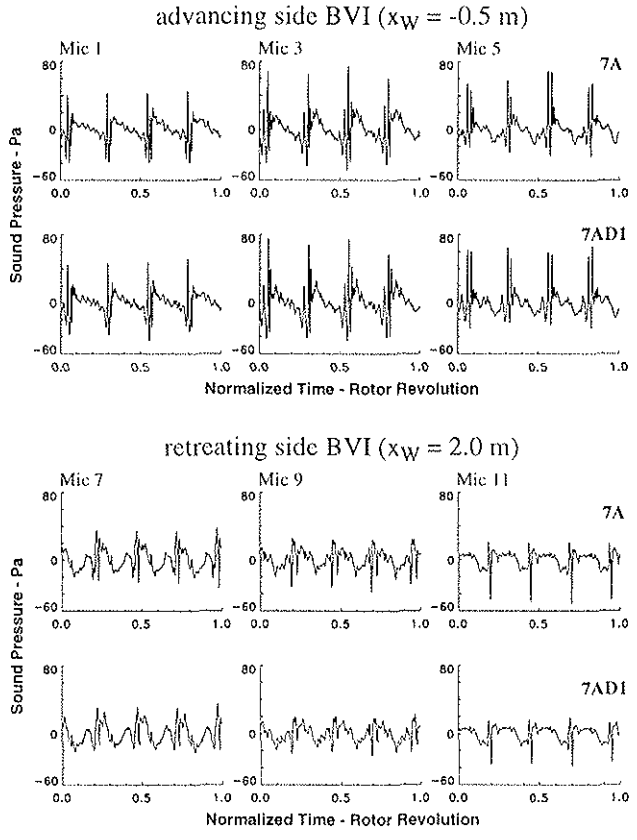

Fig. 7 Comparison of BVI noise time signatures for 7A and 7AD1 rotor at nominal descent condition (-6 degrees and 35 m/s)

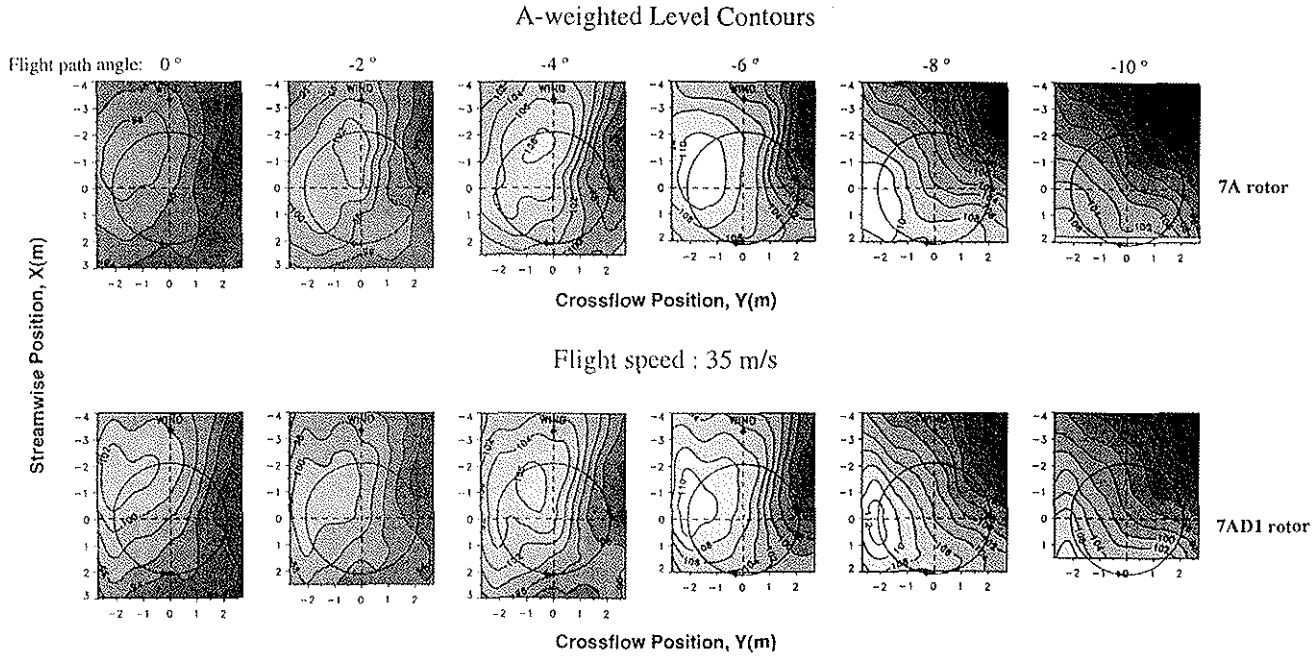

Fig. 8 Change of BVI noise radiation characteristics with flight path angle at 35 m/s flight speed for 7A and 7AD1 rotor

Data Quality Assessment

The stability and steadiness of the test conditions as well as the consistency and repeatability of the measurement results were checked and verified, to ensure a high quality standard of the measured aerodynamic and acoustic data. Reflection test results from the HELINOISE test with a similar set-up could be used to verify the anechoic test environment and to identify possible areas in the acoustic measuring plane that might be affected by acoustic shielding (Ref. 7). To ensure a proper signal to noise ratio background noise measurements at different wind speeds were performed.

Acoustic Results

Thrust Variation at Hover Condition

Although for the hover tests the shaft angle was set to -15^{0} in order to avoid disturbing rotor wake effects and to minimize recirculations, both the instantaneous and the averaged acoustic time signatures still indicate unsteady inflow effects due to recirculation.

For hover the in-plane noise radiation is most important. Figure 6 (a) shows the comparison of in-plane sound pressure time histories for the 7A and the 7AD1 rotor at hover condition with different thrust settings. Whereas at nominal thrust the blade passage frequency amplitudes for both tip shapes are nearly identical, at higher thrust these amplitudes are seen clearly reduced for the 7AD1 rotor. Figure 6 (b) shows the comparison of the A-weighted levels for the same conditions, demonstrating that the A-weighted levels are generally about 4 dB reduced for the 7AD1 rotor compared to the 7A rotor. However, the A-weighted levels include mid-frequency noise from interactions of the blades with recirculations normally not characteristic for hover.

Flight- Path and Flight-Speed Variations at Descent Condition

In Figure 7 the measured sound pressure time histories of the two different tip shapes are compared for the nominal BVI descent condition (6° descent at 35 m/s) at a microphone traverse position of X_W = -1 m (upstream of the hub) showing typical advancing side BVI (part (a)) and at a position of X_W = +2 m with typical retreating side BVI (part (b)). The comparison of the 7A and the 7AD1 rotor results show only small differences in the noise signatures.

Figure 8 illustrates the influence of the flight path variation for the 7A and 7AD1 rotor on the noise radiation contours. In general the noise radiation patterns of both rotors show similar tendencies. Only at level flight and at small descent angles the maximum radiation spot for the 7AD1 rotor is seen displaced more outboard. In both cases the advancing side maximum is shifted downstream with increasing descent angle and the maximum BVI noise is observed at a flight path angle of -8 degrees. The noise directivity characteristics for the 7A and the 7AD1 rotor are rather similar to each other. The level contours of the nominal descent condition for the 7A and the 7AD1 rotor show a distinct radiation maximum resulting from BVI on the advancing side. A retreating side BVI maximum is not seen although in the downstream measured time histories the typical negative pressure peaks from retreating side BVI are visible (Figure 7). Probably the retreating side maximum is lo-

cated more downstream beyond the measuring plane; this may also have been the case for the advancing side BVI maximum at 10° descent.

The maximum noise levels show also only small differences between the 7A and 7AD1 rotor. This is more clearly demonstrated in Figure 9 where the maximum and the spatial averaged A-weighted levels from the array as well as the A-weighted level of the nozzle microphone are compared for different flight path angles. The averaged noise levels and the nozzle microphone levels of the advanced 7AD1 rotor are seen about 1 - 2 dB lower compared to the 7A rotor at descent angles with typical BVI. The maximum noise level of the 7AD1 rotor is seen decreased only for small descent angles. At higher descent angles between 8 and 10 degrees the maximum level is even slightly increased. At level flight the A-weighted level is even distinctly increased for the 7AD1 rotor compared to the 7A rotor. It appears that the noise radiation of the 7AD1 rotor at level flight is dominated by blade-vortex interactions in the blade-tip region; this is substantiated by comparing the noise directivity plots for both rotors at level flight in Figure 8. Obviously, because of the swept back/anhedral tip shape a more parallel interaction occurs in the tip region with more intense noise radiation as compared to the rectangular tip shape. These considerations have been confirmed by the analysis of the blade pressure data.

In Figure 10 the A-weighted levels of the flight-speed variation are compared for both rotors at constant 6° descent BVI noise condition. The maximum noise level is observed at 35 m/s flight speed for the 7A rotor and at 40 m/s for the 7AD1 rotor. A noise benefit for the 7AD1 rotor is seen at lower flight speeds whereas at higher flight speeds the maximum noise levels for the 7AD1 rotor are slightly increased for this BVI condition, which is not the case for the spatial averaged dB(A) levels.

Flight-Speed and Tip-Speed Variations at Level Flight

Figure 11 compares the in-plane radiated A-weighted levels for the different rotors at level flight as function of the flight speed. The results for both rotors are close together in the mid-speed regime. Whereas at low speed (35 m/s) the noise level of the 7AD1 rotor is even increased (reason as discussed before) at higher speeds a benefit of about 2 dB can be observed for this rotor.

The expected and verified noise benefit of the 7AD1 rotor at high-speed operation is clearly visible when the in-plane sound pressure time histories for different flight speeds, as shown in Figure 12, are compared. Increasing negative peaks with increasing flight speed are seen as well as distinctly lower negative pressure peaks for the advanced rotor compared to the standard-tip rotor.

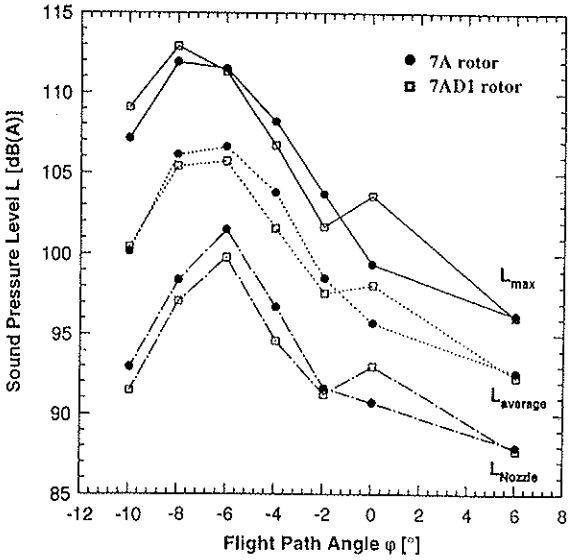

Fig. 9 Comparison of A-weighted sound levels as a function of flight path angle at constant (35 m/s) flight speed for the 7A and 7AD1 rotor

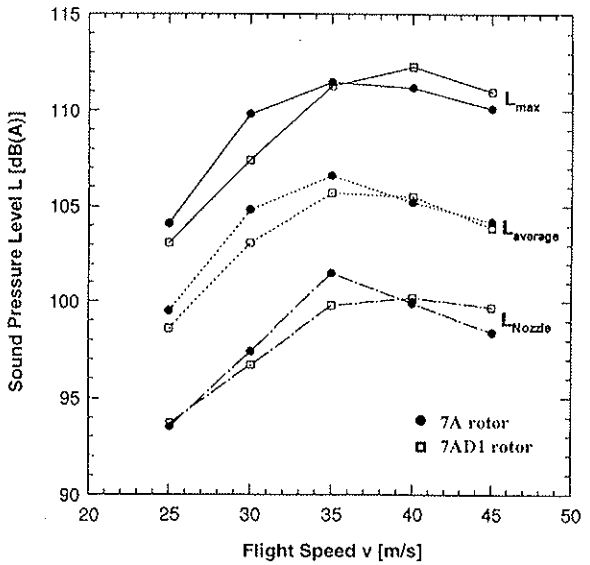

Fig. 10 Comparison of the 7A and 7AD1 rotor A-weighted sound levels as a function of flight speed at constant 6 degrees descent (BVI) condition

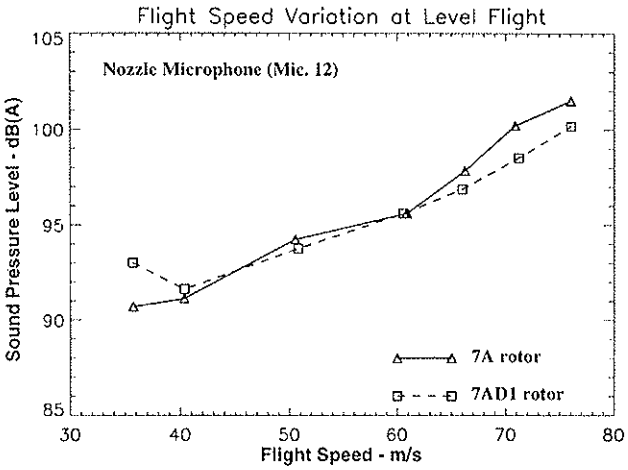

Fig. 11 Comparison of in-plane measured A-weighted sound levels for the 7A and 7AD1 rotor at level flight as function of flight speed

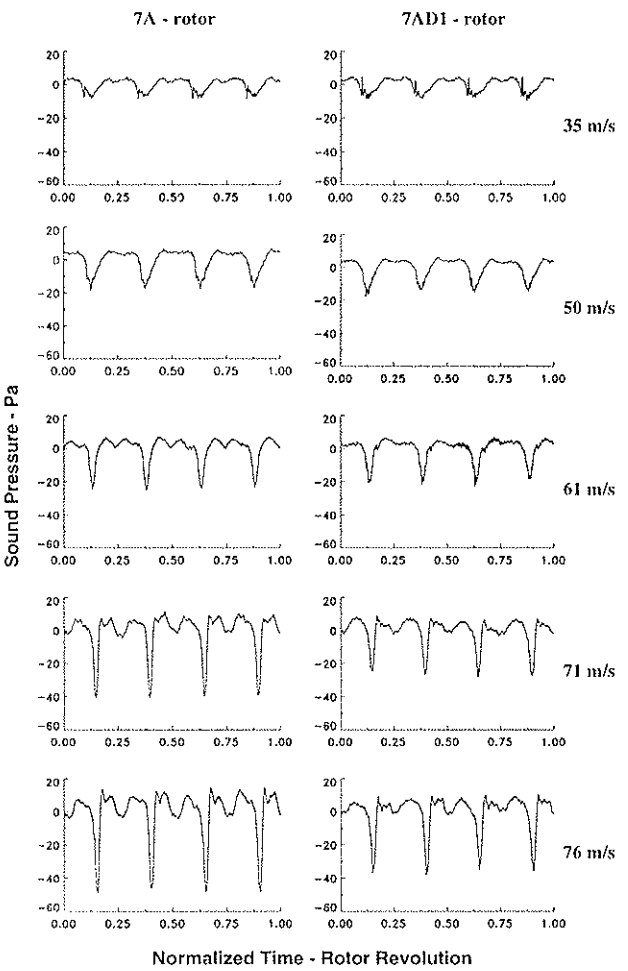

Fig. 12 Comparison of 7A and 7AD1 in-plane noise signatures (mic. 12) at level flight with different flight speeds

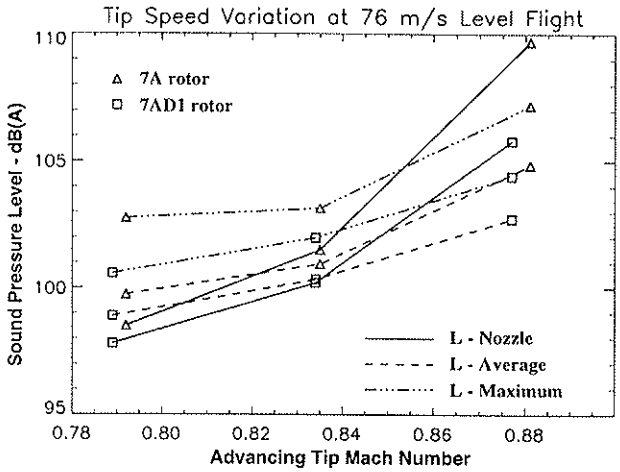

Fig. 13 Comparison of 7A and 7AD1 in-plane A-weighted sound levels as a function of the advancing tip Mach number at 76 m/s level flight, C_T = const.

Figure 13 shows the result of a tip-speed variation with all other parameters fixed. The nearly in-plane radiated A-weighted noise levels together with the maximum and averaged levels of the acoustic array for the 7A and the 7AD1 rotor are compared for three different advancing side tip Mach numbers for a level flight condition with the maximum tested flight speed of 76 m/s. Unfortunately, the tip-speed variations were performed at constant thrust coefficient. Thus, the tip-speed variation was combined with a variation in rotor thrust. Nevertheless, a clear trend of exponentially increasing A-weighted levels with increasing advancing side tip-speed can be observed for the in-plane noise radiation. Furthermore, a growing noise benefit with increased tip-speeds of the advanced tip shape (7AD1) compared with the standard tip-shape (7A) is illustrated.

Aerodynamic Results

The most important features of the parametric variations which were found in the acoustic data should also be observed in the blade pressure data. The influence of the rotor parametric variations on the blade pressures and the differences between the 7A and the 7AD1 rotor are demonstrated for some selected examples.

Hover

Because of considerable unsteady content of the blade pressures also observed at hover condition, the chordwise pressure distributions are compared for azimuthal averages. As mentioned before, even with the negative shaft angle setting of -15 degrees during the hover tests no substantial improvement was obtained concerning the recirculation effects compared to the HELINOISE test with zero degree shaft angle (Ref. 7).

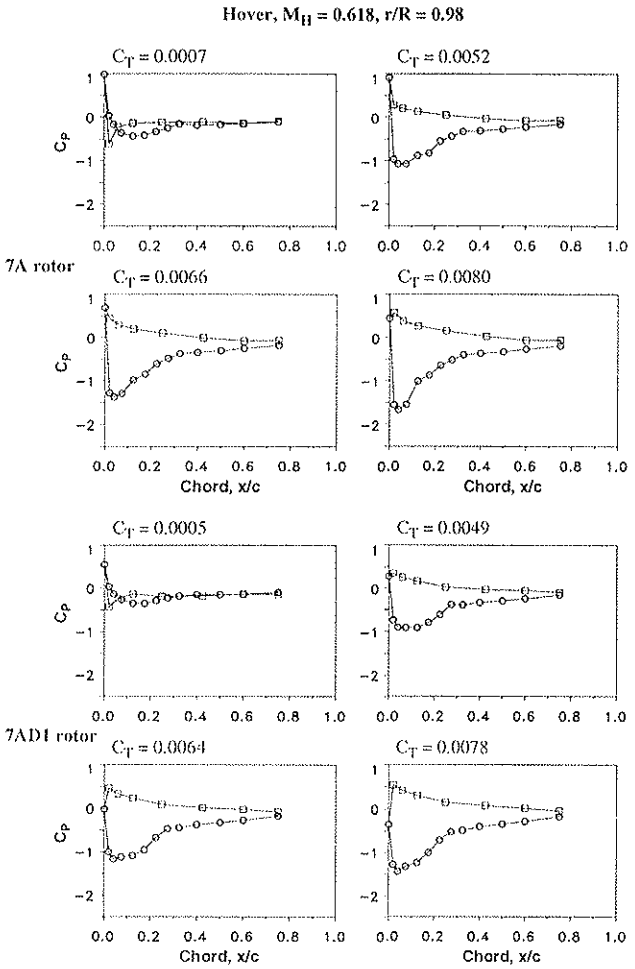

Fig. 14 Comparison of averaged chordwise blade pressure distributions for 7A and 7AD1 rotor at hover with different thrust settings (r/R = 0.98)

Figure 14 shows a comparison of the chordwise blade pressure (C_p) distribution for the 7A and the 7AD1 rotor at hover condition with different thrust settings.(C_T = 0.0005, 0.005, 0.0068 and 0.008) at the radial station r/R = 0.975. The increasing C_p difference between upper and lower side with increasing thrust setting is obvious for both tip shapes. At close inspection the chordwise C_p distribution on the upper surface shows different characteristics for the 7AD1 rotor compared to the 7A rotor at this radial station with different tip shapes; at the inner radial stations with identical airfoil profiles almost no differences have been found.

Descent Flight with BVI

In Figure 15 samples of unsteady azimuthal blade pressure distributions at 3 different radial stations (r/R = 0.7, 0.82 and 0.92) and 8 different chordwise positions (x/c = 0.02 ..... 0.75) are compared for the nominal descent condition (6° descent at 35 m/s) with typical BVI. For more clearness of the presentation only the fluctuating (AC) part of the upper side blade pressure histories are displayed.

The BVI-typical fluctuations on the advancing and on the retreating side are most pronounced near the leading edge, but, also visible up to the trailing edge, however, with much smaller amplitude. The comparison of the 7A and 7AD1 results shows only small differences in this case similar to the corresponding acoustic results and it can be concluded that the advanced tip shape has only minor effects on BVI noise.

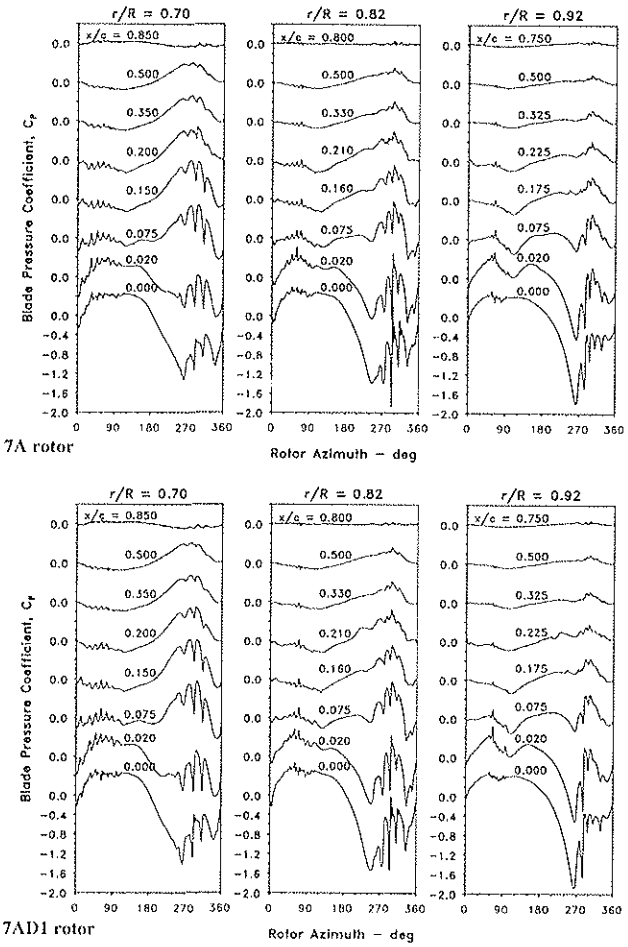

Fig. 15 Comparison of upper surface blade pressure signatures of the 7A and 7AD1 rotor at different chordwise stations and 3 radial sections for 6 degrees descent flight condition at 35 m/s (AC part only)

A comprehensive and illustrative representation of the total unsteady blade pressure information is provided by plotting isobar contours of the high-pass filtered (> 6/rev) ΔC_p distribution in the rotor plane measured near the leading edge at x/c = 0.02. In Figure 16 such differential pressure contours for the 7A and the 7AD1 rotor at the nominal descent condition (6° descent at 35 m/s) are compared. The strong blade pressure fluctuations in the 1st and 4th quadrant responsible for advancing side and retreating side BVI noise, are nicely illustrated. Comparing the results for both rotors only marginal differences can be recognized.

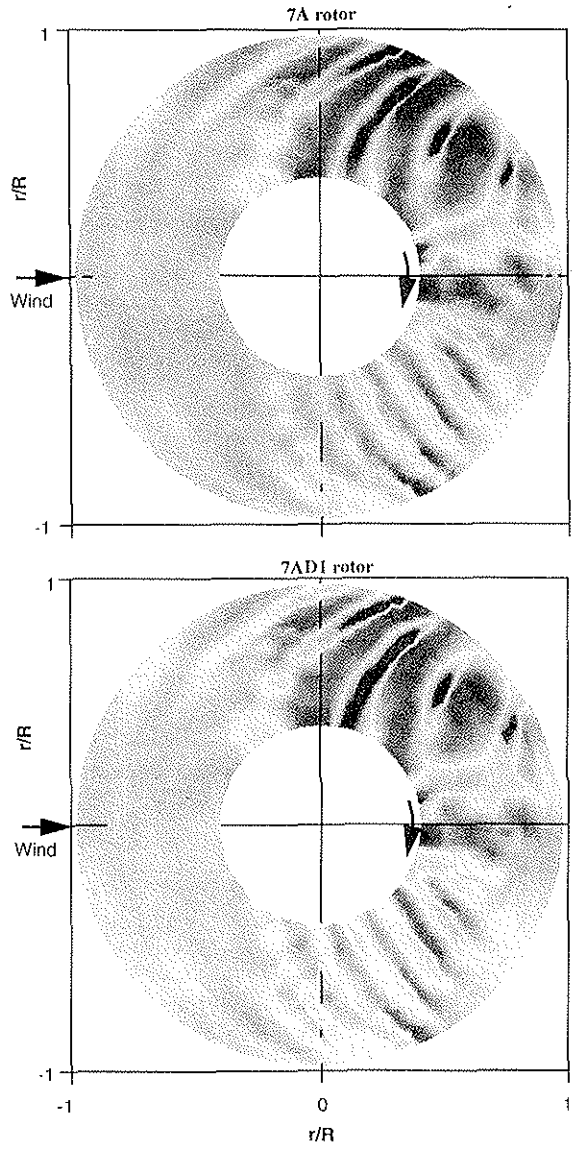

Fig. 16 Comparison of azimuthal/radial differential pressure distributions of the leading edge sensors at 2% chord for 7A and 7AD1 rotor at 6 degrees descent and 35 m/s

The influence of the descent angle on the radiated noise can also be demonstrated using such high-pass filtered differential pressure contours. In Figure 17 the pressure contours for different descent conditions for the 7A rotor are compared starting at level flight. For level flight the most intense blade-vortex interactions occur mainly in the 2nd and 3th quadrant with oblique interactions. With increasing descent angle the BVI region is moved more and more downstream into the 1st and 4th quadrant and finally for the highest descent angle towards the downstream end of the rotor plane where the BVI intensities are largely reduced. For BVI noise generation the nearly parallel blade-vortex interactions in the middle-range of the 1st and 4th quadrant are most important. This explains that maximum BVI noise radiation is observed for the descent angle range between 6 and 8 degrees. Similar observations can be made for the 7AD1 rotor. The pressure contours for level flight offer an explanation for the increased BVI noise radiation at level flight of the 7AD1 rotor compared to the 7A rotor as presented above. The BVI noise is caused by an interaction near the blade tip in the azimuthal range around 80 degrees. With the swept back/anhedral tip shape the interaction near the tip is more parallel and thus the noise radiation is increased compared to the rectangular tip shape of the 7A rotor.

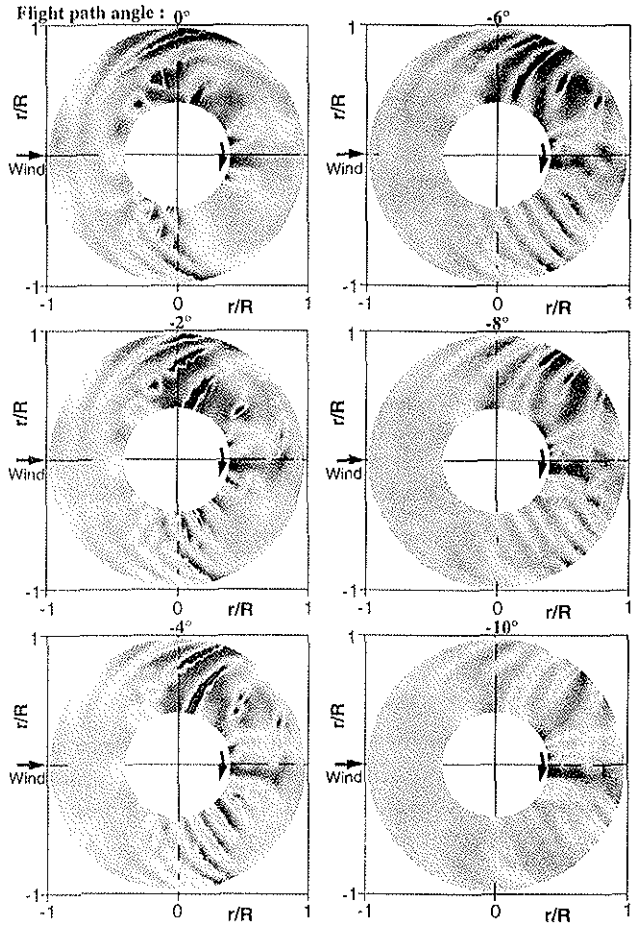

Fig. 17 Change of the instationary azimuthal/radial pressure distribution at leading edge with descent angle (7A rotor)

Moderate High-Speed Level Flight

In Figure 18 a similar representation of the unsteady blade pressure histories is shown as in Figure 15, but for a moderate high-speed level flight at 76 m/s, the highest tunnel speed tested. The advancing tip Mach number is 0.835. For the 7A rotor at certain chord locations (0.10 - 0.35 c) on the advancing blade and in the azimuthal range between 30 and 120 degrees supersonic pockets are observed caused by supersonic flow and shock formation with rapid changes in the chordwise and azimuthal C_p distribution. Such supersonic flow regions are seen reduced for the 7AD1 rotor, especially at the radial station near the blade tip (r/R = 0.975). As expected and also observed regarding the acoustic results, the advanced tip shape is especially beneficial for high-speed noise reduction.

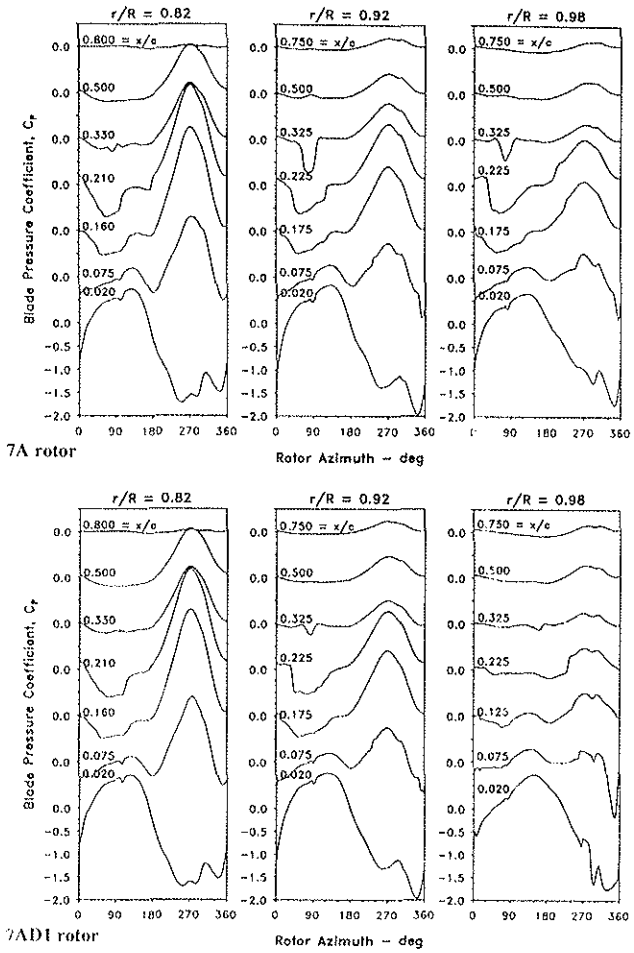

Fig. 18 Comparison of upper surface blade pressure signatures of the 7A and 7AD1 rotor at different chordwise stations and 3 radial sections for high-speed level flight at 76 m/s

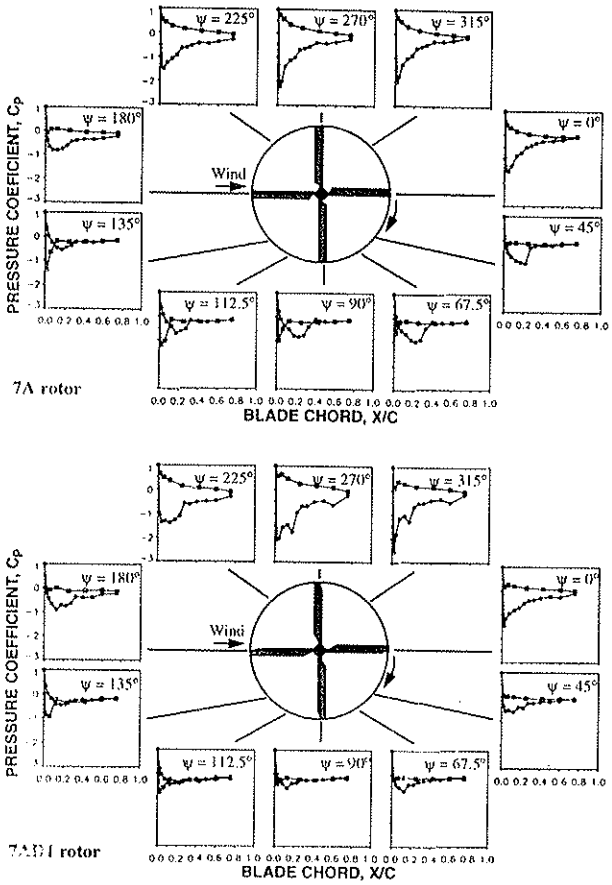

Fig. 19 Typical chordwise blade pressure distributions for the 7A and 7AD1 rotor at various blade azimuth locations for high-speed level flight at 76 m/s

In Figure 19 the chordwise C_p distributions of the 7A and the 7AD1 rotor for the same moderate high-speed case at different azimuthal locations and at the radial station near the blade tip (r/R = 0.975) are compared. For the 7A rotor extended supersonic flow regions and shock formations are visible on the advancing side of the rotor plane between 45 and 135 degrees while subsonic flow prevails on the retreating side. The supersonic flow region has nearly vanished for the 7AD1 rotor.

LLS Flow Visualization Results

Descent Condition

Illustrative qualitative results of the LLS flow visualization are video recording images of cross sections through any desired blade tip vortex which was properly seeded with oil smoke and illuminated by the laser light sheet.

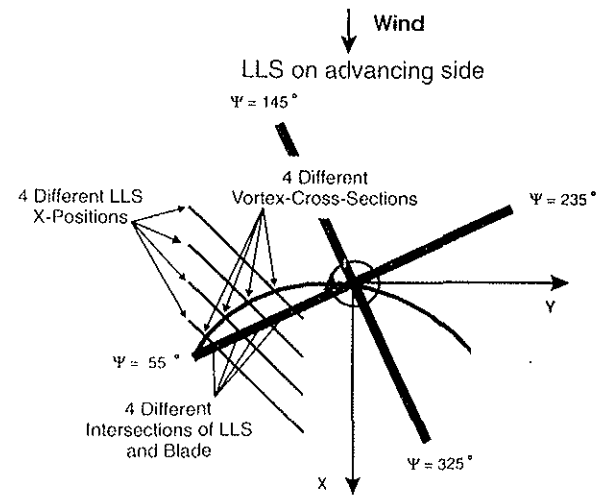

Fig. 20 Application of the LLS technique at BVI condition

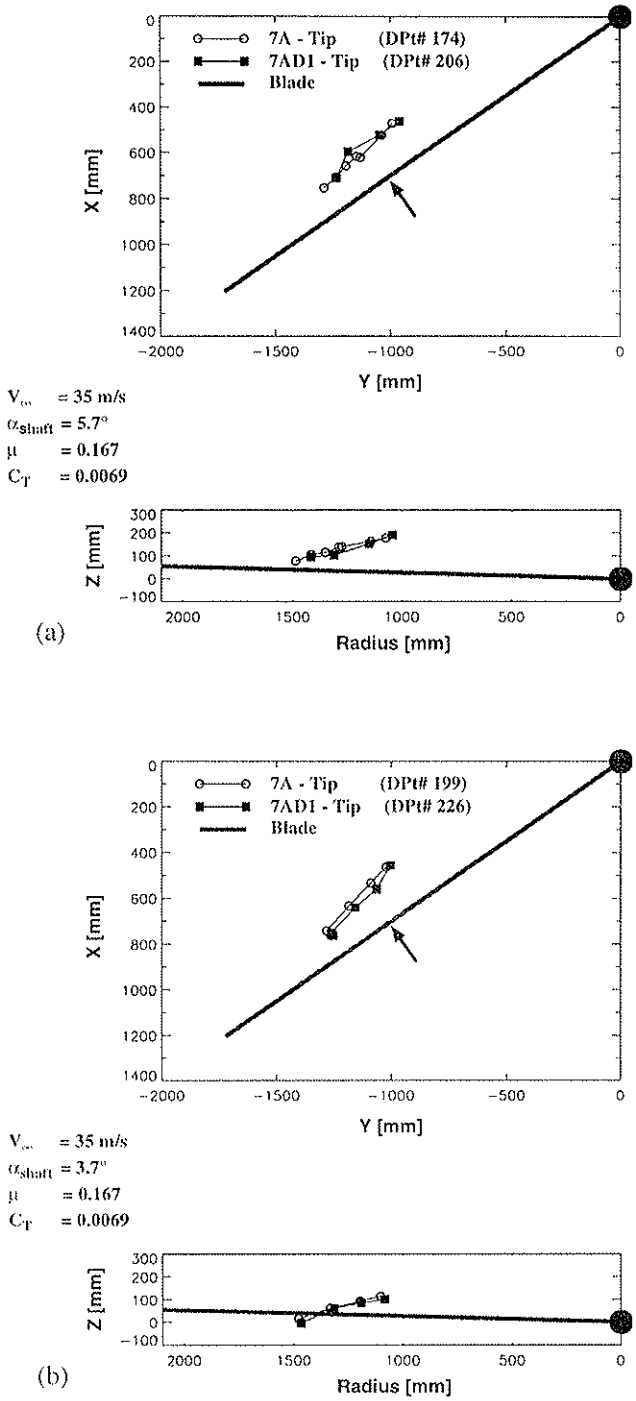

Fig. 21 Vortex trajectories determined by LLS-technique at a blade position of 55 degrees azimuth for descent flight conditions, (a) at 6 degrees descent, (b) at 4 degrees descent condition

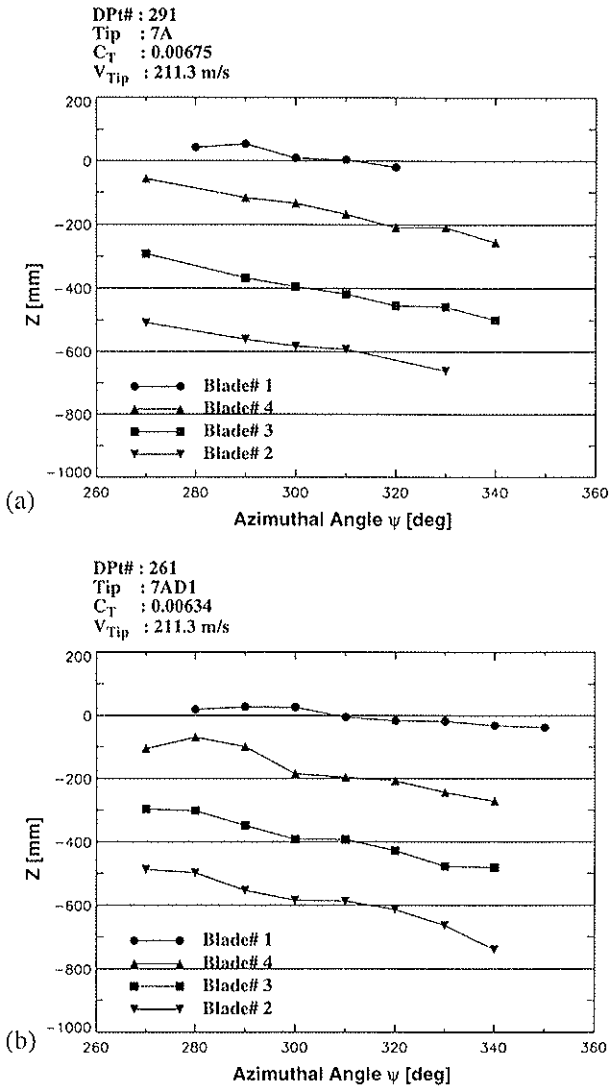

Fig. 22 Vortex trajectories at nominal hover condition, (a) 7A rotor, (b) 7AD1 rotor

Quantitative results have been accomplished from measuring the vortex core centres in space of several discrete sections along the vortex of interest as illustrated in Figure 20. In the HELISHAPE test four discrete sections of the most important vortex were measured which was most significant for BVI on the advancing side.The blade position was fixed at 55 degrees azimuth. LLS measurements were performed for different low speed descent cases. Figure 21 (a) shows the results for both rotors for a descent angle of 6 degrees and Figure 21 (b) those for a descent angle of 4 degrees. In the top views, the Z-axis represents the vertical axis of the wind tunnel, X- and Y-axis define a horizontal plane in which the measured blade position as well as the measured tip-vortex segments are plotted. In the side views (frontal to the blade) the Z-axis represents the rotor shaft axis and the R-axis the blade span. The vertical distance between the blade and the vortices provides an estimate for the "miss distance".

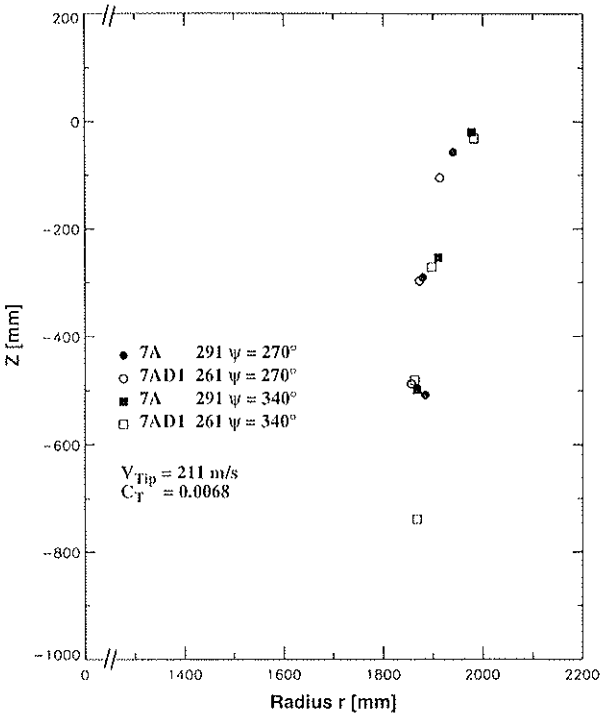

Fig. 23 Tip vortex positions at hover condition in a vertical plane at 270 degrees azimuth

Obviously, the tip-vortex segments for the 7A and the 7AD1 rotor are close together. The top views indicate that the blade position of 55 degrees is nearly in the middle of the azimuth range in which the blade-vortex interaction occurs. Concerning the 6 degrees descent case, the side view shows that the measured vortex segment is above the rotor. An extrapolation of the vortex path in tip direction indicates an interaction in the outer blade-span region. At the 4 degrees descent case the interaction takes place more inboard and therefore is less intense.

Hover Condition

At hover condition the vortex core positions of four vortices could be determined in the azimuthal range from 270 degrees up to about 340 degrees. Figure 22 presents results for the 7A rotor (part (a)) and for the 7AD1 rotor (part (b)) for a hover case with nominal C_T and nominal tip-speed. For each rotor the vertical tip-vortex displacement (Z) is plotted versus azimuth angle ψ representing vortex age. The slope of the vortex paths is an indication for the downwash velocity. The comparison of the 7A and 7AD1 vortices shows only marginal differences. The downwash velocity for the 7AD1 rotor appears to be slightly lower than for the 7A rotor.

Finally, in Figure 23 the tip vortex core positions measured for different blade azimuth locations of 270 and 340 degrees are shown. The measurements were actually conducted in a vertical plane at 270 degrees azimuth with the reference blade at 270 and 340 degrees azimuth, respectively. The contraction of the rotor wake or more specifically of the blade-tip vortices is clearly illustrated.

Concluding Remarks

Within the framework of the rotor aeroacoustic HELISHAPE programme, a major cooperative research initiative between 16 European partners, a parametric model rotor wind tunnel test was successfully completed. The experimental task of the HELISHAPE programme - parametric wind tunnel tests - was defined in order to generate a high quality database for the validation of aerodynamic and aeroacoustic prediction codes and for assessment of noise palliatives. Within HELISHAPE rotor blades of advanced airfoil design and two exchangeable blade tips were chosen for investigation. For a large matrix of test conditions the aerodynamic blade surface pressure distribution and the related acoustic pressure field along with blade dynamic characteristics were simultaneously measured. By application of laser light sheet flow visualization additional information pertaining to blade-tip vortex geometry and blade-vortex miss distance was obtained.

The results of the two different tip shapes were compared and the trends of the most important parameter variations were discussed. The aeroacoustic improvements of the 7AD1 blade compared to the rectangular 7A tip were investigated with respect to Blade-Vortex Interaction (BVI) noise and with respect to High Speed (HS) noise.

Maximum BVI noise radiation was determined for both rotors at low speed 8 degrees descent (35m/s), whereas the spatial averaged BVI noise levels showed maximum values at 6 degrees descent.

A BVI noise benefit of about 1-2 dB was measured for the advanced 7AD1 rotor compared to the 7A rotor at certain descent angles while for high-speed in-plane noise radiation a noise benefit of 1 - 4 dB was determined.

Application of the LLS flow visualization technique provided informative insight into the blade-tip vortex geometry at descent and hover conditions important for the improvement of aerodynamic prediction codes.

In summary, a very comprehensive aerodynamic and acoustic data base was measured together with wind tunnel, rotor performance, and blade dynamic data covering hover, descent, and level flight conditions for a model rotor of advanced design with two different tip shapes. The high quality aeroacoustic data base obtained provides the basis to validate the computational methods developed or improved by the theoretical research effort within the HELISHAPE project. An extensive analysis of the data will further the physical understanding and the prediction capability of helicopter rotor impulsive noise.

Acknowledgements

The HELISHAPE project was generously sponsored by the European Union. The EU Project Monitor was Mr. J. M. Martin-Hernandez. The Industrial Project Manager was Dr. V. Kloeppel of ECD.

Special thanks go to the Management and the Technical Support Team of the German-Dutch Wind Tunnel, DNW,

and in particular to Dr. E. Mercker and Mr. K. Pengel for providing the LLS flow visualization technique.

Last not least the authors would like to offer their sincere thanks to the engineers and technicians of the DLR-Institutes of Flight Mechanics and of Design Aerodynamics (both Braunschweig) and of Aeroelasticity (Goettingen) for their tireless efforts in preparation and conduct of this highly complex HELISHAPE test.

References

1. Boxwell, D. A.; Schmitz, F. H.; Splettstoesser, W. R.; Schultz, K.-J.: "Model Helicopter Rotor High Speed Impulsive Noise: Measured Acoustics and Blade Pressures", NASA TM 85850 and US-AAVRAD-COM TR-A-14, September 1983

2. Splettstoesser, W. R.; Schultz, K.-J.; Boxwell, D. A.; Schmitz, F. H.: "Helicopter Model Rotor Blade/Vortex-Interaction Impulsive Noise, Scalibility and Parametric Variations", Proceedings 10th European Rotorcraft Forum, The Hague, August 1984 and NASA TM 86007, TM-84-A-7

3. Zinner, R. A.; Boxwell, D. A.; Spencer, R. H.: "Review and Analysis of the DNW/Model 360 Rotor Acoustic Data Base", 15th European Rotorcraft Forum, Amsterdam, September 1989

4. Yu, Y. H.; Landgrebe, A. J.; Liu, S. R.; Lorber, P. F.; Jordan, D. E.; Pollack, M. J.; Martin, R. M.: "Aerodynamic and Acoustic Test of a United Technologies Model Scale Rotor at DNW", Proceedings pp. 1233-1250, American Helicopter Society 46th Annual Forum, Washington DC, May 1990

5. Martin, R. M.; Splettstoesser, W. R.; Elliot, J. W.; Schultz, K.-J.: "Advancing Side Directivity and Retreating Side Interactions of Model Rotor Blade Vortex Interaction Noise", NASA Tech. Paper 2784 and AVSCOM Technical Report 87-B-3, 1988

6. Schultz, K.-J.; Splettstoesser, W. R.: "Model Tail Rotor Noise Study in the DNW - Measured Acoustics, Blade Pressures, Noise Predictions -", Paper No. 78, Proceedings, 18th European Rotorcraft Forum, Avignon, September 1992

7. Splettstoesser, W.; Junker, B.; Schultz, K.-J.; Wagner, W.; Weitemeyer, W.; Protopsaltis, A.; Fertis, D. : "The HELINOISE Aeroacoustic Rotor Test in the DNW - Test Documentation and Representative Results", DLR-Mitt. 93 - 09, 1993

8. Seidel, M.; Maarsingh, R. A.: "Test Capabilities of the German-Dutch Wind Tunnel DNW for Rotors, Helicopters and V/STOL Aircraft", Proceedings of the 5th European Rotorcraft and Powered Lift Aircraft Forum, September 1979

9. Van Ditshuizen, J. C. A.; Courage, G. D.; Ross, R.; Schultz K.-J.: "Acoustic Capabilities of the German-Dutch Wind Tunnel (DNW)", AIAA-83-0146, Jan. 1983

10. Stephan, M.; Klöppel, V.; Langer, H.-J.: "A New Wind Tunnel Test Rig for Helicopter Testing", Paper No. 66, 14th European Rotorcraft Forum, September 1988

11. Mercker, E.; Pengel, K.: "Flow Visualization of Helicopter Blade-Tip Vortices", Paper No. 26, Proceedings 18th European Rotorcraft Forum, Avignon, September 1992

12. Gelhaar, B.; Junker, B.; Wagner, W.: "DLR-Rotor Teststand Measures Unsteady Rotor Aerodynamic Data", Paper No. C 8, Proceedings 19th European Rotorcraft Forum, Cernobbio, Italy, September 1993

13. Breustedt, W. (SCITRAN, transl.): "Data Analysis on the Rotor Test Stand Program for Interactive Processing", NASA TM-77948, 1985

14. Brooks, T. F.; Jolly, R. J.; Marcolini M. A.: "Determination of Noise Source Contributions Using Scales Model Rotor Acoustic Data", NASA TP 2825, 1988